Hybrid Structure of Static Var Compensator and Hybrid Active Power Filter (SVC//HAPF) for Medium-Voltage Heavy Loads Compensation

Lei Wang, Chi-Seng Lam, *Senior Member, IEEE*, and Man-Chung Wong, *Senior Member, IEEE*

***Abstract*—In this paper, the structure, modeling, parameter design, and control method are proposed for a new hybrid structure of a static var compensator in parallel with a hybrid active power filter (SVC//HAPF). The SVC part of the SVC//HAPF is used to dynamically compensate the reactive power. And, the HAPF part is used to provide harmonic power and small amount of reactive power compensation. Due to the large fundamental voltage drop on coupling the *LC* part, the active inverter part of the SVC//HAPF has low voltage rating. Meanwhile, the parallel-connected SVC acts as a current divider to reduce the active inverter current. Therefore, the proposed SVC//HAPF shows the great promise in compensating harmonic current and wide-range reactive power with a low (both) voltage and current rating active inverter part. To show the advantages of the proposed SVC//HAPF, simulation comparisons among the active power filter (APF), HAPF, SVC in series with HAPF (SVC−HAPF), and the proposed SVC//HAPF are provided. Finally, experimental results based on the laboratory-scaled hardware prototype are given to show the validity of the SVC//HAPF.**

***Index Terms*—Active power filter (APF), harmonic current compensation, hybrid APF (HAPF), reactive power compensation, static var compensator (SVC).**

I. Introduction

LOW power factor (PF) and current harmonic distortion are considered as two of the major power quality problems in three-phase three-wire medium-voltage-level power system.

Manuscript received April 25, 2017; revised July 8, 2017 and September 25, 2017; accepted October 20, 2017. Date of publication November 13, 2017; date of current version February 13, 2018. This work was supported in part by the Science and Technology Development Fund, Macao SAR (FDCT), under Grant 025/2017/A1 and Grant 109/2013/A3 and in part by the Research Committee of the University of Macau under Grant MYRG2015-00009-FST, Grant MRG012/WMC/2015/FST, and Grant MYGR2017-00038-FST. *(Corresponding author: Chi-Seng Lam.)*

L. Wang is with the Department of Electrical and Computer Engineering, Faculty of Science and Technology, University of Macau, Macao 999078, China.

C.-S. Lam is with the State Key Laboratory of Analog and Mixed Signal VLSI, University of Macau, Macao, China (e-mail: C.S.Lam@ieee.org; cslam@umac.mo).

M.-C. Wong is with the Department of Electrical and Computer Engineering, Faculty of Science and Technology, University of Macau, Macao, China, and also with the State Key Laboratory of Analog and Mixed Signal VLSI, University of Macau, Macao, China.

Color versions of one or more of the figures in this paper are available online at http://ieeexplore.ieee.org.

Digital Object Identifier 10.1109/TIE.2017.2772201

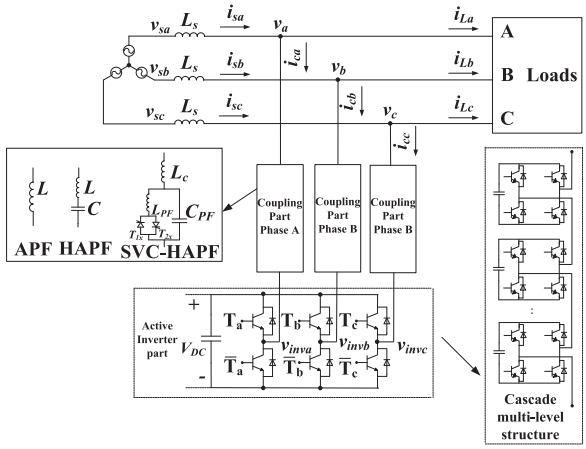

Fig. 1. Structures of conventional APF, HAPF, and SVC–HAPF.

The static var compensators (SVCs) are traditionally used to dynamically compensate reactive power. However, the SVCs have many inherent problems, such as resonance problems, poor harmonic compensation ability, and slow response [1], [2]. To overcome these inherent problems, the active power filters (APFs) for power quality compensation have drawn much attention since 1976. However, during the operation of APFs, the active inverter part requires high voltage rating. Therefore, the APFs require costly multilevel structure for medium-voltage-level applications [3]–[5], as shown in Fig. 1, thereby limiting their widespread applications. To reduce the voltage rating (cost) of the active inverter part, an *LC* coupling hybrid APF (HAPF) has been proposed in 2003. Even though the large *LC* impedance can reduce the inverter part voltage rating, it also limits the compensating range of the HAPFs [6], [7]. In 2003, Dixon *et al.* [8] proposed the combined system of SVC in parallel with APF (SVC//APF). The SVC part of this structure is used to compensate most of the reactive power; thus, the current rating of the APF can be significantly reduced. However, the voltage rating of the APF is still high so that the SVC//APF still requires costly multilevel structure for medium-voltage-level applications. In 2012, Luo *et al.* [9] proposed a novel hybrid system, which consists of a thyristor-controlled reactor (TCR) and a resonant impedance-type HAPF (RITHAPF) (TCR//RITHAPF). The RITHAPF part is an APF crossing over a matching transformer connected in parallel with a fundamental series resonant circuit. As most

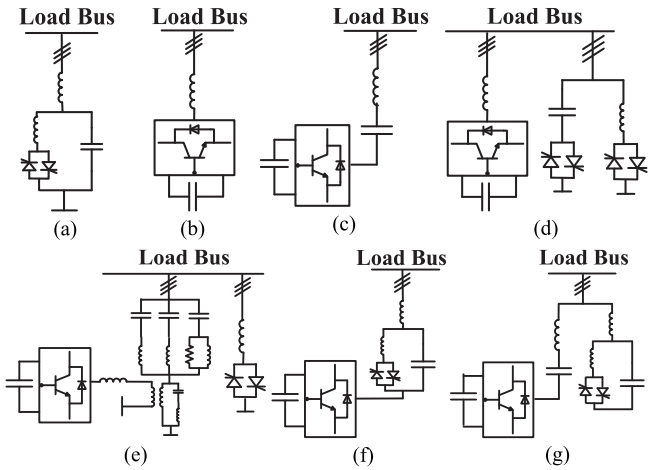

Fig. 2. Simplified circuit configurations of (a) SVC [1], [2]; (b) APF [3]–[5]; (c) HAPF [6], [7]; (d) SVC//APF [8]; (e) TCR//RITHAPF [9]; (f) SVC–HAPF [10]–[18]; and (g) proposed SVC//HAPF.

of the loads are inductive and the TCR part is also inductive, the required capacitive compensating current generated by the RITHAPF part should be larger in order to count in the TCR part. Due to this reason, the current rating of the RITHAPF part can be high for heavy loads compensation. In addition, the high-current-rating-matching transformer in TCR//RITHAPF can also significantly drive up the system cost. In 2014, the hybrid structures of SVC in series with APF (SVC–HAPFs) are proposed in [10]–[18]. The SVC–HAPF has the characteristics of wide reactive power compensation range and low voltage rating of the active inverter part. However, during heavy loads compensation, the current rating of the SVC–HAPF can be high. In this paper, a hybrid structure of an SVC in parallel with an HAPF (SVC//HAPF) are proposed for medium-voltage heavy loads compensation. The proposed SVC//HAPF not only has a wide reactive power compensation range, but also obtains both low voltage and current inverter ratings. As the cost of the SVC part is much lower than that of the active inverter part, the reduction of active inverter rating (voltage and current) can lead to a decrease in the total cost of the SVC//HAPF system. Therefore, the total cost of the hybrid structure SVC//HAPF can be significantly reduced for medium-voltage-level heavy loads compensation.

The simplified circuit configurations the aforementioned power quality compensators are provided in Fig. 2. And, the comparisons among different power quality compensators in terms of reactive power compensation range, inverter voltage and current ratings and cost for medium-voltage heavy loads compensation are summarized in Table I. In the table, more asterisks represent wider reactive power compensation range, larger inverter current rating, larger inverter voltage rating, and higher cost.

In the following Section II, the circuit configuration and modeling of the three-phase three-wire SVC//HAPF are presented. Then, the parameter design of the SVC//HAPF is introduced in Section III. After that, the control strategy of the SVC//HAPF is proposed in Section IV. In order to show the advantages of the proposed SVC//HAPF, the simulation comparisons among the APF, HAPF, SVC–HAPF and SVC//HAPF are provided in

TABLE I
COMPARISONS AMONG DIFFERENT POWER QUALITY COMPENSATORS IN TERMS OF REACTIVE POWER COMPENSATION RANGE, INVERTER VOLTAGE RATING, CURRENT RATING, AND COST

	Year	Reactive Power Compensation Range	Inverter Current Rating	Inverter Voltage Rating	Cost
SVC [1], [2]	1960s	****	–	–	*
APF [3]–[5]	1976	****	***	****	****
HAPF [6], [7]	2003	*	***	**	**
SVC//APF [8]	2003	*****	*	****	****
TCR//RITHAPF [9]	2012	***	**	**	****
SVC–HAPF [10]–[18]	2014	****	***	**	***
SVC//HAPF	2017	****	*	**	***

Note: The shade area means the undesirable characteristic.

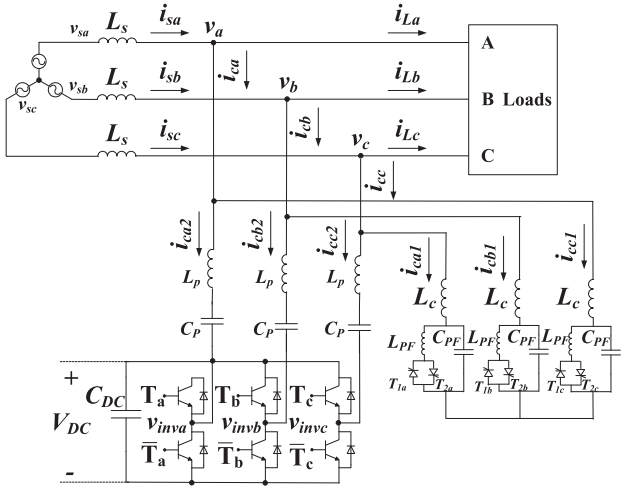

Fig. 3. Circuit configurations of the SVC//HAPF.

Section V. In Section VI, representative experimental results are given based on a laboratory-scaled hardware prototype. Finally, conclusion is drawn in Section VII.

II. CIRCUIT CONFIGURATION AND MODELING OF THE THREE-PHASE SVC//HAPF

The circuit configuration of a three-phase three-wire SVC//HAPF is provided in Fig. 3, where v_{sx}, v_x, and $v_{\mathrm{inv}x}$ are the source voltage, the load voltage, and the inverter voltage, respectively. The subscript x denotes phase $x = a, b, c$; i_{sx}, i_{Lx}, and i_{cx} are the source current, the load current, and the compensating current, respectively. The SVC part of the SVC//HAPF consists of a coupling inductor L_c, a parallel capacitor C_{PF}, and a TCR with an inductor L_{PF}. And the SVC part can be both star and delta connections. The HAPF part consists of a coupling LC filter (L_p and C_p), a two-level voltage-source inverter (VSI), and a dc-link capacitor C_{DC}. The VSI of the HAPF part has both low voltage rating (due to large fundamental voltage drop on the coupling LC and low current rating due to the current divider between i_{cx1} and i_{cx2}.

The single-phase modeling for the SVC//HAPF is proposed in Fig. 4. At the fundamental frequency [see Fig. 4(a)], the

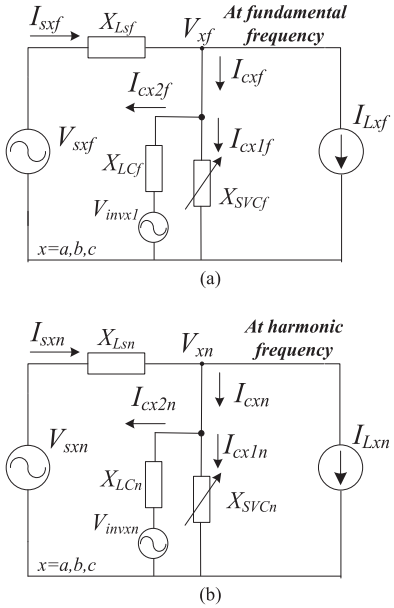

Fig. 4. Single-phase SVC//HAPF modeling: (a) at fundamental frequency and (b) at harmonic frequency.

coupling *LC* filter are used to compensate a fixed amount of reactive power, while the SVC part impedance $X_{\mathrm{SVC}f}$ is used to dynamically compensate the reactive power difference between the *LC* filter and the loads by controlling its firing angle. Ideally, the fundamental inverter voltage $V_{\mathrm{inv}xf}$ can be designed close to zero, as it is not necessary to compensate the fundamental reactive power. At the harmonic frequency [see Fig. 4(b)], the harmonic inverter voltage $V_{\mathrm{inv}xn}$ is used to compensate the loading harmonic current.

In the following, the steady-state compensation analysis and the parameter design of the SVC//HAPF is proposed according to Fig. 4.

III. Parameter Design of SVC//HAPF

In this section, a parameter design method is discussed and explained in three parts. In Section III-A, the parameter design of $C_{\mathrm{PF}}, L_{\mathrm{PF}}$, and C_P is proposed under the fundamental frequency consideration. In Section III-B, the parameter design of the dc-link voltage V_{DC} is proposed under harmonic frequency consideration. In Section III-C, the design of L_c and L_p is given.

A. Design of $C_{\mathrm{PF}}, L_{\mathrm{PF}}$, and C_P Under Fundamental Frequency Consideration

At the fundamental frequency [see Fig. 4(a)], $X_{\mathrm{SVC}f}$ and $X_{\mathrm{LC}f}$ are used to compensate the load-required fundamental reactive power. Therefore, the fundamental inverter voltage $V_{\mathrm{inv}xf}$ can be kept minimized as zero because it is not necessary to compensate the fundamental reactive power.

Referring to Fig. 4(a), the SVC//HAPF fundamental impedance ($X_{\mathrm{SVC}f}$ and $X_{\mathrm{LC}f}$) can be calculated by applying the Ohm's law as

$$\frac{X_{\mathrm{LC}f}\cdot X_{\mathrm{SVC}f}(\alpha_x)}{X_{\mathrm{LC}f}+X_{\mathrm{SVC}f}(\alpha_x)}=\frac{V_{xf}}{I_{cxf}}=\frac{V_{xf}^2}{Q_{Lx}} \tag{1}$$

where V_{xf}, I_{cxf}, and Q_{Lx} are the fundamental load voltage, compensating current and the load reactive power, respectively, where x stands for phase a, b, and c. $X_{\mathrm{LC}f}$ and $X_{\mathrm{SVC}f}$ are the fundamental impedances of the SVC part and the coupling *LC* part of the HAPF. And $X_{\mathrm{LC}f}$ and $X_{\mathrm{SVC}f}$ can be expressed as

$$X_{\mathrm{LC}f}=\omega\cdot L_p-1/\omega\cdot C_p \tag{2}$$

$$X_{\mathrm{SVC}f}(\alpha_x)=\frac{\pi X_{L_{\mathrm{PF}}}X_{C_{\mathrm{PF}}}}{X_{C_{\mathrm{PF}}}(2\pi-2\alpha_x+\sin 2\alpha_x)-\pi X_{L_{\mathrm{PF}}}}+X_{L_c}. \tag{3}$$

In (3), $\omega\,(=2\pi f)$ is the angular frequency, $X_{Lc}, X_{C\mathrm{PF}}$, and $X_{L\mathrm{PF}}$ are the fundamental impedances of L_c, C_{PF}, and L_{PF}, respectively. α_x is the firing angle of the thyristor. The SVC part has two back-to-back connected thyristors (T_{1x}, T_{2x}) and they are triggered alternately in every half cycle. When $\alpha_x=180^\circ$ (thyristors are opened for the whole cycle), the SVC part has the maximum capacitive SVC impedance $X_{\mathrm{SVC}f}\ (\alpha_x=180^\circ)(<0)$. On the other hand, when the firing angle $\alpha_x=90^\circ$ (one of the thyristors is closed for the whole cycle), the SVC part has the minimum inductive SVC impedance $X_{\mathrm{SVC}f}(\alpha_x=90^\circ)$. Therefore, $X_{\mathrm{SVC}f}\ (\alpha_x=180^\circ)$ and $X_{\mathrm{SVC}f}\ (\alpha_x=90^\circ)$ can be expressed as

$$X_{\mathrm{SVC}f}(\alpha_x=180^\mathrm{o})=X_{L_c}-X_{C_{\mathrm{PF}}}=\omega L_c-1/\omega C_{\mathrm{PF}} \tag{4}$$

$$X_{\mathrm{SVC}f}(\alpha_x=90^\mathrm{o})=\frac{X_{L_{\mathrm{PF}}}X_{C_{\mathrm{PF}}}}{X_{C_{\mathrm{PF}}}-X_{L_{\mathrm{PF}}}}+X_{L_c}=\frac{\omega L_{\mathrm{PF}}}{1-\omega^2 L_{\mathrm{PF}}C_{\mathrm{PF}}}+\omega L_c. \tag{5}$$

Based on (1)–(5), the relationship between the load-required inductive and capacitive reactive power and the SVC//HAPF components value can be expressed as

$$\frac{V_{xf}^2}{Q_{Lx(\mathrm{MaxCap})}}=X_{\mathrm{SVC}f}(\alpha_x=90^\mathrm{o})//X_{\mathrm{LC}f}\approx\frac{\omega L_{\mathrm{PF}}}{1-\omega^2 L_{\mathrm{PF}}(C_{\mathrm{PF}}+C_P)} \tag{6}$$

$$\frac{V_{xf}^2}{Q_{Lx(\mathrm{MaxInd})}}=X_{\mathrm{SVC}f}(\alpha_x=180^\mathrm{o})//X_{\mathrm{LC}f}\approx\frac{1}{\omega(C_{\mathrm{PF}}+C_p)} \tag{7}$$

where $Q_{Lx(\mathrm{MaxInd})}$ and $Q_{Lx(\mathrm{MaxCap})}$ are, respectively, the maximum load-required inductive power and capacitive reactive power. In (6) and (7), the impedances of L_c and L_p are ignored due to their small values (will discussed in part *C*). By satisfying (6) and (7), $C_{\mathrm{PF}}, L_{\mathrm{PF}}$, and C_p can be designed as

$$C_{\mathrm{PF}}+C_p=\frac{Q_{Lx(\mathrm{MaxCap})}}{\omega V_{xf}^2} \tag{8}$$

$$L_{\mathrm{PF}}=\frac{V_x^2}{\omega\cdot Q_{Lx(\mathrm{MaxCap})}+\omega^2 V_{xf}^2\,(C_{\mathrm{PF}}+C_p)}. \tag{9}$$

$C_{\mathrm{PF}}, L_{\mathrm{PF}}$, and C_p can be designed from (8) and (9).

B. Design of V_{DC} Based on Harmonic Frequency Analysis

Referring to the harmonic model given in Fig. 4(b), the harmonic current I_{sxn} circulating in the source is provided as

$$I_{sxn} = \frac{X_{\mathrm{SVC//HAPF}n}}{\mathrm{X}_{Lsn} + X_{\mathrm{SVC//HAPF}n}} \cdot I_{Lxn} \tag{10}$$

where the subscript n represents each harmonic order, I_{sxn} and I_{Lxn} are the source and load harmonic currents, $X_{\mathrm{SVC//HAPF}n}$ is the harmonic equivalent impedance of SVC//HAPF, which can be expressed as

$$\begin{aligned} X_{\mathrm{SVC//HAPF}n} &= X_{\mathrm{SVC}n} // (X_{\mathrm{LC}n} + V_{\mathrm{inv}xn} / I_{\mathrm{cx2}n}) \\ &= \frac{X_{\mathrm{SVC}n} \cdot [X_{\mathrm{LC}n} + (V_{\mathrm{inv}xn} / I_{cx2n})]}{X_{\mathrm{SVC}n} + X_{\mathrm{LC}n} + V_{\mathrm{inv}xn} / I_{cx2n}}. \end{aligned} \tag{11}$$

In (11), the purpose of the inverter voltage $V_{\mathrm{inv}xn}$ is to adjust the equivalent harmonic impedance of the SVC//HAPF to be zero $(X_{\mathrm{SVC//HARF}n} \approx 0)$ so that the load harmonic current will not pollute the source side. According to (11), the inverter voltage $V_{\mathrm{inv}xn}$ at the harmonic frequency can be given as

$$|V_{\mathrm{inv}xn}| = |X_{\mathrm{LC}n} \cdot I_{cx2n}| = \left| \frac{X_{\mathrm{LC}n} \cdot X_{\mathrm{SVC}n}}{|X_{\mathrm{LC}n}| + |X_{\mathrm{SVC}n}|} \cdot I_{Lxn} \right|. \tag{12}$$

In (12), the harmonic impedance of X_{LCn} and $X_{\mathrm{SVC}n}$ at each n can be expressed as

$$X_{LCn} = n\omega \cdot L_p - 1/n\omega \cdot C_p \tag{13}$$

$$\begin{aligned} &|X_{\mathrm{SVC}n}(\alpha_x)| \\ &= \left| \frac{\pi(n\omega L_{\mathrm{PF}})}{(2\pi - 2\alpha_x + \sin 2\alpha_x) - \pi(n\omega)^2 \cdot L_{\mathrm{PF}} C_{\mathrm{PF}}} + n\omega L_c \right|. \end{aligned} \tag{14}$$

Finally, the dc-link voltage V_{DC} can be calculated as

$$\begin{aligned} V_{\mathrm{DC}} > \sqrt{6}\sqrt{\sum_{n=2}^{\infty} V_{\mathrm{inv}xn}^2} = \Bigg(&\sqrt{6}\sqrt{\sum_{n=2}^{\infty} V_{\mathrm{inv}an}^2}, \\ &\sqrt{6}\sqrt{\sum_{n=2}^{\infty} V_{\mathrm{inv}bn}^2}, \sqrt{6}\sqrt{\sum_{n=2}^{\infty} V_{\mathrm{inv}cn}^2} \Bigg)_{\max} \end{aligned} \tag{15}$$

where $V_{\mathrm{inv}xn}$ can be obtained from (12) that is designed based on worst case I_{Lxn}. And the information of I_{Lxn} can be obtained by measuring the loading for a period of time before the design of SVC//HAPF. The final V_{DC} is designed to be larger than the maximum value among each phase (15).

C. Design of L_p and L_c for Harmonic Order Tuning

The purpose of L_p is to provide a low LC impedance at the most dominated harmonic order, so that the required dc-link voltage for harmonic compensation can be reduced. The value of L_p can be designed as

$$L_p = \frac{1}{(2\pi f n_1)^2 C_P} \tag{16}$$

where n_1 is the dominated harmonic order (e.g., $n_1 = 5$), f is the system frequency.

The thyristors for each phase of the SVC part can be considered as a pair of bidirectional switches that generate low-order harmonic currents when the thyristors change states. The purpose of the design of L_c is to tune the possible generated harmonic current order to diverge from the characteristic harmonic orders $n_d = 6n \pm 1\mathrm{th}$ $(n = 1, 2, 3, \ldots)$ of a three-phase three-wire power system to avoid the SVC harmonic current generation problem [2]. Based on the transient analysis in [2], the harmonic orders generated by the SVC part can be given as

$$n_2 = \frac{1}{2\pi f \sqrt{L_c C_{\mathrm{PF}}}} \tag{17}$$

$$n_3 = \frac{1}{2\pi f} \sqrt{\frac{L_c + L_{\mathrm{PF}}}{L_c L_{\mathrm{PF}} C_{\mathrm{PF}}}} \tag{18}$$

where the harmonic orders n_2 and n_3 mainly depend on L_c, L_{PF}, and C_{PF} values. And, L_c can be expressed as

$$L_c = \frac{1}{(2\pi f n_2)^2 C_{\mathrm{PF}}} \qquad L_c = \frac{1}{(2\pi f n_3)^2 C_{\mathrm{PF}} - 1/L_{\mathrm{PF}}}. \tag{19}$$

For a three-phase three-wire system, there is no $3n\mathrm{th}$ order harmonic current and the common harmonic orders are $6n \pm 1(\geq 5)$ with $n = 1, 2, 3 \ldots$. To avoid the harmonic currents injection by the SVC, it is suggested to tune n_2 and n_3 to be away from the $6n \pm 1\mathrm{th}$ order and/or close to $3n\mathrm{th}$ order.

IV. Control Strategy of SVC//HAPF

In this section, the control strategy of the SVC//HAPF is separated into three parts: 1) the SVC part; 2) the HAPF part; and 3) the overall control block (see Fig. 5).

A. SVC Part Control

According to (1), the required SVC impedance can be calculated through $X_{\mathrm{LC}f}, Q_{Lx}$, and V_{xf}

$$X_{\mathrm{SVC}f}(\alpha_x) = \frac{V_{xf}^2 \cdot X_{\mathrm{LC}f}}{Q_{Lx} \cdot X_{\mathrm{LC}f} - V_{xf}^2} \tag{20}$$

where $X_{\mathrm{LC}f}$ is fundamental impedance of coupling LC in HAPF, and $X_{\mathrm{LC}f}$ is a fixed value as shown in (2). The Q_{Lx} and V_{xf} are the load reactive power and load voltage, which can be calculated in real-time as

$$\begin{bmatrix} q_{La} \\ q_{Lb} \\ q_{Lc} \end{bmatrix} = \begin{bmatrix} v_a \cdot i_{\mathrm{La}}^D - v_a^D \cdot i_{La} \\ v_b \cdot i_{Lb}^D - v_b^D \cdot i_{Lb} \\ v_c \cdot i_{Lc}^D - v_c^D \cdot i_{Lc} \end{bmatrix} \tag{21}$$

$$\mathrm{V}_{xf} = \|v\|/\sqrt{3} = \sqrt{v_a^2 + v_b^2 + v_c^2} \Big/ \sqrt{3} \tag{22}$$

where v_x^D and i_{Lx}^D can be obtained by delaying v_x and i_{Lx} by a phase angle of 90°. q_{Lx} is the phase instantaneous reactive power. Then $Q_{Lx} \approx -\bar{q}_{Lx}/2$ can be obtained by passing q_{Lx} in (21) through low-pass filters (LPFs). $\|v\|$ is the norm of three-phase instantaneous load voltage.

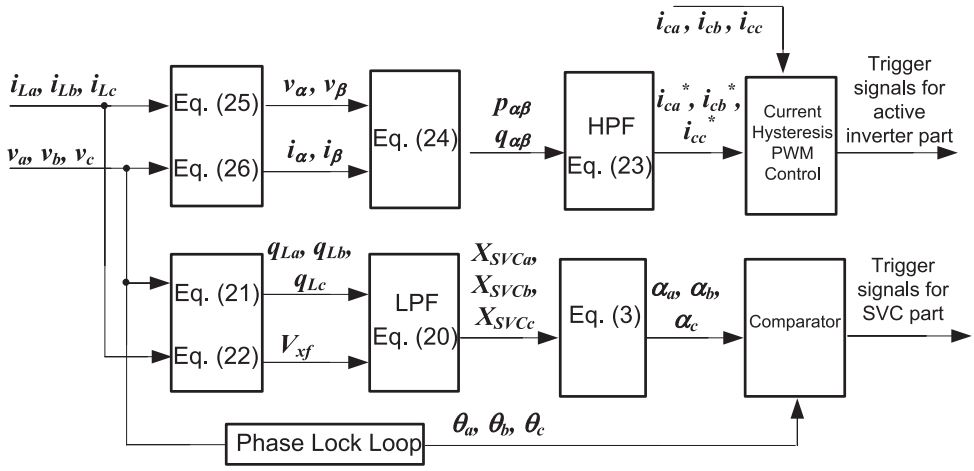

Fig. 5. Overall control strategy of the SVC//HAPF.

After obtaining Q_{Lx} and V_{xf}, the required $X_{\mathrm{SVC}f}$ can be obtained from (20). With the calculated $X_{\mathrm{SVC}f}$, the firing angle α_x can be calculated through (3). However, (3) does not have a closed-form solution. A lookup table (LUT) has been installed to directly obtain the firing angle α_x with the known $X_{\mathrm{SVC}f}$. By comparing the firing angle α_x with the phase angle of the load voltage θ_x, which can be obtained by using phase-locked loop (PLL).

B. HAPF Part Control

As the instantaneous power theory [19] is chosen to calculate the reference compensating current i_{cx}^*. The calculated i_{cx}^* contains the harmonics, reactive power and unbalanced power. By controlling the compensating current i_{cx} to track its reference i_{cx}^*, the active inverter part can compensate the load harmonic currents and improve the reactive power compensation ability and dynamic performance of the SVC part. i_{cx}^* can be calculated through the well-known instantaneous p–q theory [19] as

$$\begin{bmatrix} i_{ca}^* \\ i_{cb}^* \\ i_{cc}^* \end{bmatrix} = \sqrt{\frac{2}{3}} \cdot \frac{1}{v_\alpha^2 + v_\beta^2} \begin{bmatrix} 1 & 0 \\ -1/2 & \sqrt{3}/2 \\ -1/2 & -\sqrt{3}/2 \end{bmatrix} \cdot \begin{bmatrix} v_\alpha & -v_\beta \\ v_\beta & v_\alpha \end{bmatrix} \cdot \begin{bmatrix} \tilde{p}_{\alpha\beta} \\ q_{\alpha\beta} \end{bmatrix} \tag{23}$$

where $p_{\alpha\beta}$ and $q_{\alpha\beta}$ are, respectively, the instantaneous active power and reactive power, which include dc components $\bar{p}_{\alpha\beta}$ and $\bar{q}_{\alpha\beta}$ and ac components $\tilde{p}_{\alpha\beta}$ and $\tilde{q}_{\alpha\beta}$. $\bar{p}_{\alpha\beta}$ and $\bar{q}_{\alpha\beta}$ contain the fundamental active and reactive current components, respectively, while $\tilde{p}_{\alpha\beta}$ and $\tilde{q}_{\alpha\beta}$ contain the harmonic currents and negative-sequence components. $\tilde{p}_{\alpha\beta}$ is obtained by passing $p_{\alpha\beta}$ through a high-pass filter (HPF). $p_{\alpha\beta}$ and $q_{\alpha\beta}$ can be obtained as

$$\begin{bmatrix} p_{\alpha\beta} \\ q_{\alpha\beta} \end{bmatrix} = \begin{bmatrix} v_\alpha & v_\beta \\ -v_\beta & v_\alpha \end{bmatrix} \cdot \begin{bmatrix} i_\alpha \\ i_\beta \end{bmatrix}. \tag{24}$$

In (23) and (24), the voltages (v_α and v_β) and currents (i_α and i_β) in the $\alpha - \beta$ frame are transformed from $a - b - c$ frames by

$$\begin{bmatrix} v_\alpha \\ v_\beta \end{bmatrix} = \begin{bmatrix} 1 & -1/2 & -1/2 \\ 0 & \sqrt{3}/2 & -\sqrt{3}/2 \end{bmatrix} \cdot \begin{bmatrix} v_a \\ v_b \\ v_c \end{bmatrix} \tag{25}$$

$$\begin{bmatrix} i_\alpha \\ i_\beta \end{bmatrix} = \begin{bmatrix} 1 & -1/2 & -1/2 \\ 0 & \sqrt{3}/2 & -\sqrt{3}/2 \end{bmatrix} \cdot \begin{bmatrix} i_{La} \\ i_{Lb} \\ i_{Lc} \end{bmatrix} \tag{26}$$

where v_x and i_{Lx} are, respectively, the load voltage and current signals.

C. Overall Control Block

The overall control block is provided in Fig. 5. From Fig. 5, for the SVC part control, (21) and (22) are used to calculate the load reactive power q_{Lx} and the load voltage V_{xf}. Then, the required impedance of SVC part $X_{\mathrm{SVC}f}$ can be obtained from (20). In (20), the obtained $X_{\mathrm{SVC}f}$ is to compensate the difference between the load reactive power and the reactive power provided by the coupling LC of HAPF part. After that, the corresponding firing angle α_x of the SVC part can be obtained from (3). Finally, by comparing the firing angle α_x with the phase angle of the load voltage θ_x, the trigger signals for the thyristor of the SVC can be obtained.

The purpose of the HAPF part is used to compensate the reactive power left by the SVC part and the harmonic current by limiting the compensating current i_{cx} to its reference i_{cx}^*. Through (25) and (26), the load voltage and current (v_x and i_{Lx}) in $a - b - c$ frame are transformed to $\alpha - \beta$ frame. By using the instantaneous p–q theory [19], the active power and reactive power $\alpha - \beta$ frame can be calculated through (24). With the help of the HPF and (23), the load reactive power and harmonic active power can be transferred to i_{cx}^*. In this paper, the current hysteresis pulsewidth modulation (PWM) control is applied. Compared with the voltage control PWM methods, the current hysteresis PWM control has the advantage of fast dynamic response, simplicity of implementation, high robustness, etc. Through the current hysteresis PWM control method, the trigger signals of the HAPF can be generated by comparing i_{cx} with i_{cx}^*.

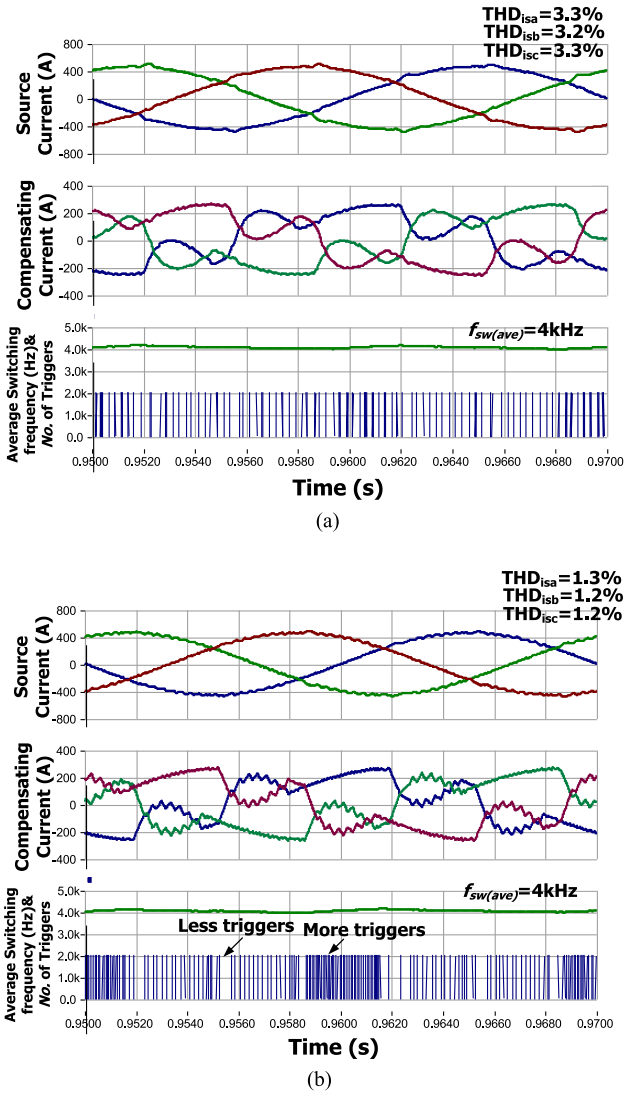

Fig. 6. Waveforms of source current, compensating current, average switching frequency, and trigger signals by using: (a) proportional gain control and (b) hysteresis band control.

V. Simulation Case Studies of Different Compensators

In this section, the simulation case studies are separated into two parts for discussion.

A. Simulation Case Studies of PWM Control

The structure of the HAPF part of the proposed SVC//HAPF was first proposed by Srianthumrong and Akagi [22]. The proportional gain control (indirect current control) was applied to control the HAPF [22], in which this control can obtain regular switching frequency. Later on, the applications of hysteresis band control (direct current control) in HAPF have been reported in [6] and [21], and this control yields irregular switching frequency. The simulation comparisons of the proportional gain control and hysteresis band control for the SVC//HAPF are provided in Figs. 6 and 7.

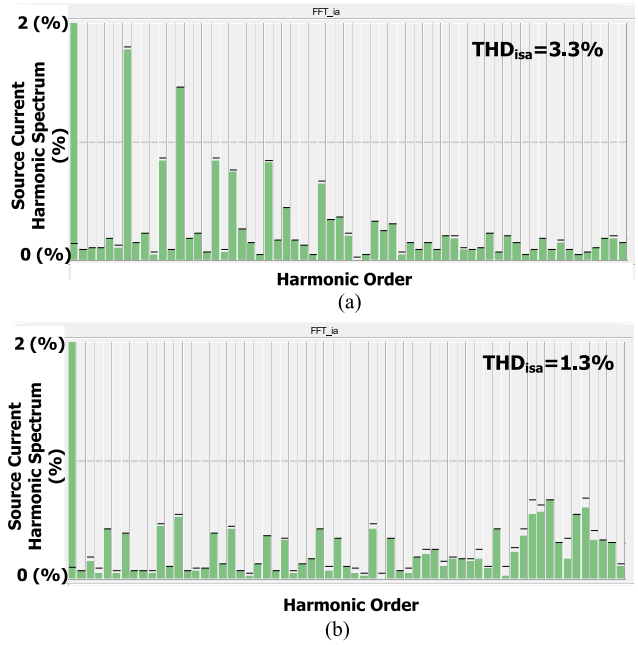

Fig. 7. Source current harmonic spectrum by using (a) proportional gain control and (b) hysteresis band control.

TABLE II
Parameter Design of SVC//HAPF for Simulation and Experimental Case Studies

Parameter	Equations	Load Condition	Designed Range	Design Values
$C_{\mathrm{PF}}, L_{\mathrm{PF}}, C_p$	(8), (9)	Q_{Lx1} = 30 kvar, Q_{Lx2} = 2200 kVar	−5.47 Mvar < Q_{Lx} < 5.83 Mvar	C_{PF} = 360 μF, L_{PF} = 9 mH, C_p = 80 μF
L_p	(16)	Compensate dominated current harmonic (5th order)	$n_1 = 5$ in (16)	L_p = 5 mH
L_c	(17)–(19)	Diverge from harmonic order $6n \pm 1$ (≥ 5)	$n_2 \approx 2.4, n_3 \approx 2.9$ in (19)	L_c = 5 mH

TABLE III
Parameters of APF, HAPF, SVC–HAPF, and SVC//HAPF Used for 10 kV Simulation Case Studies

	Parameters	Physical Values
System parameters	V_{LL}, f, L_s	10 kV, 50 Hz, 0.2 mH
APF [3]–[5]	L	5 mH
HAPF [6], [7]	L, C	5 mH, 80 μF
SVC–HAPF [10]–[18]	$L_c, L_{\mathrm{PF}}, C_{\mathrm{PF}}$	5 mH, 9 mH, 360 μF
SVC//HAPF	$L_c, L_{\mathrm{PF}}, C_{\mathrm{PF}}$ L_p, C_P	5 mH, 9 mH, 360 μF, 5 mH, 80 μF

Based on Figs. 6 and 7, it can be seen that the proportional gain control can compensate the worst phase source current THD_{isx} to 3.3%, while the hysteresis band control can compensate THD_{isx} to 1.3% performance under the same average switching frequency $f_{\mathrm{sw(ave)}} = 4\,\mathrm{kHz}$.

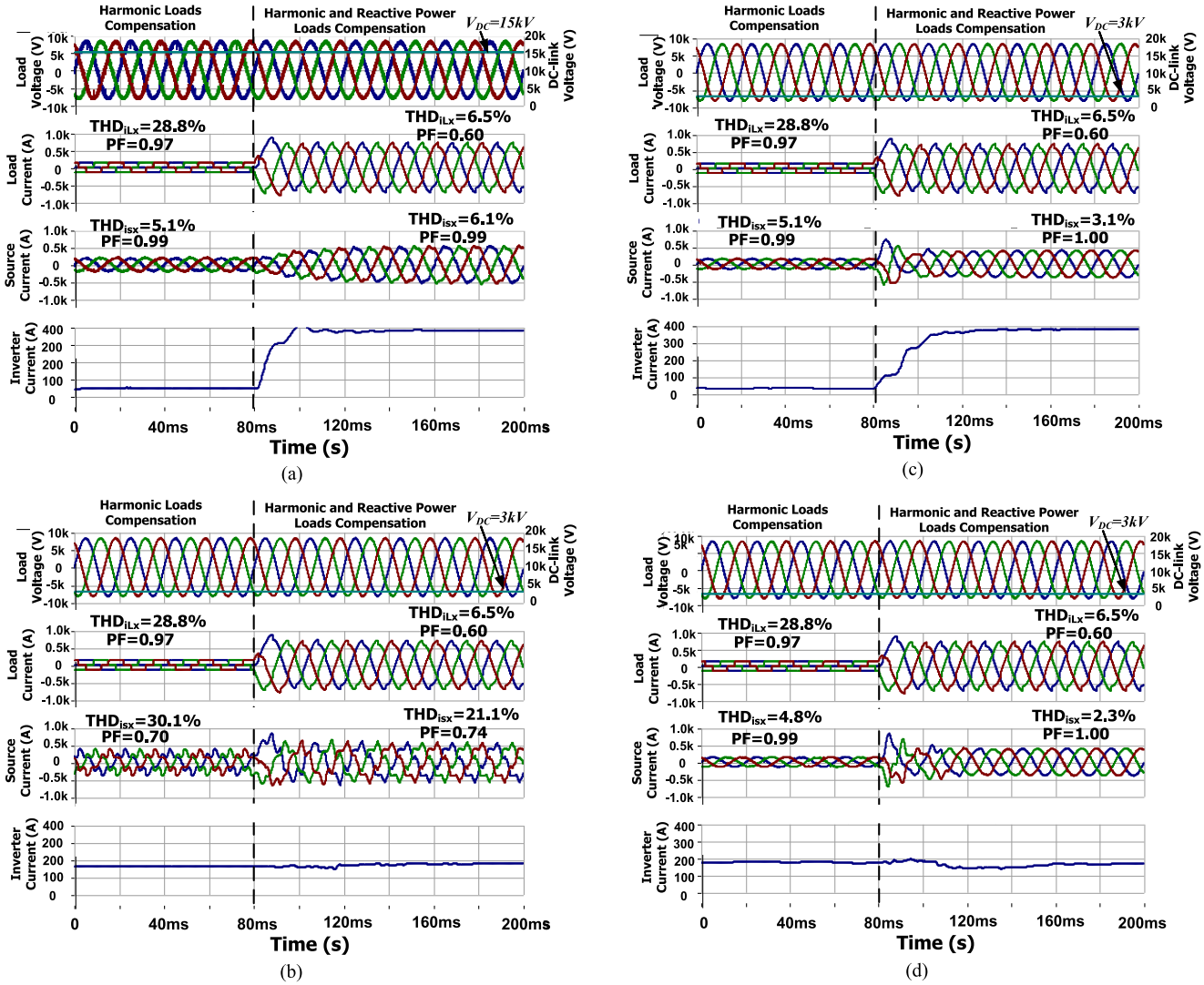

Fig. 8. Waveforms of load voltage, dc-link voltage, load current, source current, and compensating inverter current for harmonic loads current compensation ($Q_{Lx} = 0$) and harmonic and reactive power loads compensation by using: (a) APF, (b) HAPF, (c) SVC–HAPF, and (d) the proposed SVC//HAPF.

Based on the simulation results, it can prove that the hysteresis control method (irregular switching frequency) can have better performance than the proportional gain control (relative regular switching frequency) under the same average switching frequency. Thus, the hysteresis band control is selected in this paper.

B. Comparative Simulation Case Studies of APF, HAPF, SVC–HAPF, and the Proposed SVC//HAPF

The SVC//HAPF can obtain good compensation performances with low-voltage/current active inverter rating. In this section, the simulation case studies are provided to show the aforementioned advantages of the proposed SVC//HAPF in comparison with the conventional APF, HAPF, and SVC–HAPF. The parameters of the SVC//HAPF used in simulation and experimental case studies are following the proposed parameter design method in Section III. And, the summary of the SVC//HAPF parameter design is given in Table II. The parameters of different compensators for simulation case studies are given in Table III. In addition, for fair comparison, the dc-link voltages of HAPF, SVC–HAPF, and the proposed SVC//HAPF are set to be the same ($V_{\rm DC} = 3\,{\rm kV}$) in simulation case studies.

Fig. 8 shows the waveforms of load voltage, dc-link voltage, load current, source current, and compensating inverter current (i_{cx2}) for harmonic loads current compensation ($Q_{Lx} = 0$) and harmonic and reactive power loads compensation by using the APF, HAPF, SVC–HAPF, and the proposed SVC//HAPF. Table III summarizes the corresponding simulation results.

From Fig. 8(a) and Table IV, it can be seen that the APF can compensate the PF close to unity from the original 0.97 and 0.60 for the light harmonic loads and heavy inductive loads respectively. Meanwhile, the source current THD$_{isx}$ has been improved to lower than 6.5% from 28.8% of light loads and 6.5% of heavy loads. The required $V_{\rm DC}$ is 15 kV and the inverter compensating current is increasing to about 400 A for heavy inductive loads compensation.

TABLE IV
SIMULATION RESULTS FOR DIFFERENT LOADS COMPENSATION BEFORE AND AFTER APF, HAPF, SVC–HAPF, AND THE PROPOSED SVC//HAPF COMPENSATION

Loads	Comp.	Q_{sx} (var)	PF	i_{sx} (A)	THD_{vx} (%)	THD_{isx} (%)	V_{DC} (V)
Light Harmonic Loads	Before Comp.	30 k	0.97	110	1.0	28.8	–
	APF	7 k	0.99	120	0.6	5.1	15k
	HAPF	−820 k	0.70	210	0.7	30.1	3k
	SVC–HAPF	5 k	0.99	113	0.5	5.1	3k
	SVC//HAPF	4 k	0.99	112	0.6	4.8	3k
Heavy inductive loads	Before Comp.	2200 k	0.60	473	1.0	6.5	–
	APF	9 k	1.00	321	0.5	6.1	15 k
	HAPF	1290 k	0.74	342	0.7	21.1	3k
	SVC–HAPF	6 k	1.00	274	0.6	3.1	3 k
	SVC//HAPF	4k	1.00	289	0.6	2.3	3k

From Fig. 8(a) and Table IV, it can be seen that the APF can compensate the PF close to unity from the original 0.97 and 0.60 for the light harmonic loads and heavy inductive loads respectively. Meanwhile, the source current THD_{isx} has been improved to lower than 6.5% from 28.8% of light loads and 6.5% of heavy loads. The required V_{DC} is 15 kV and the inverter compensating current is increasing to about 400 A for heavy inductive loads compensation.

From Fig. 8(b) and Table IV, the HAPF only provides a fixed amount of capacitive reactive power, so that the PF is getting worse for light harmonic loads compensation. The PF has been compensated from 0.97 and 0.60 to 0.70 and 0.74 for the light harmonic loads and heavy inductive loads, respectively. The source current THD_{isx} has been compensated to 30.1% and 21.1%, which are not satisfactory. Even though the HAPF requires low V_{DC} $(= 3\,\text{kV})$ and low fixed-inverter compensating current (about 150 A), the HAPF cannot obtain good compensation performance.

Based on Fig. 8(c) and Table IV, SVC–HAPF can improve the PF and THD_{isx} to about unity and lower than 5.5% for both light harmonic and heavy inductive loads. The required V_{DC} is 3 kV, and the inverter compensating current is increasing to about 400 A for heavy loads compensation.

From Fig. 8(d) and Table IV, the PF has been improved to about unity from 0.97 and 0.60 after SVC//HAPF compensation. And, the source current THD_{isx} has been improved to 4.8% and 2.3% from the original 28.8% for light harmonic loads and 6.5% for heavy inductive loads compensation, respectively. In addition, the SVC//HAPF requires low dc-link voltage $(= 3$ kV) and low fixed inverter compensating current (about 150 A).

Based on the earlier discussions and simulation results, the APF requires the highest V_{DC} to compensate different loads. For APF and SVC–HAPF, the required inverter current is increasing as the required compensating reactive power is increasing. On the other hand, even though HAPF requires the low V_{DC} and low fixed inverter current as the SVC//HAPF, it obtains the poorest compensation performance. Compared with the APF, HAPF, and SVC–HAPF, the proposed SVC//HAPF requires both low V_{DC} and low inverter current to obtain satisfactory

Fig. 9. Experimental setup of the 110 V−5 kVA SVC//HAPF experimental prototype.

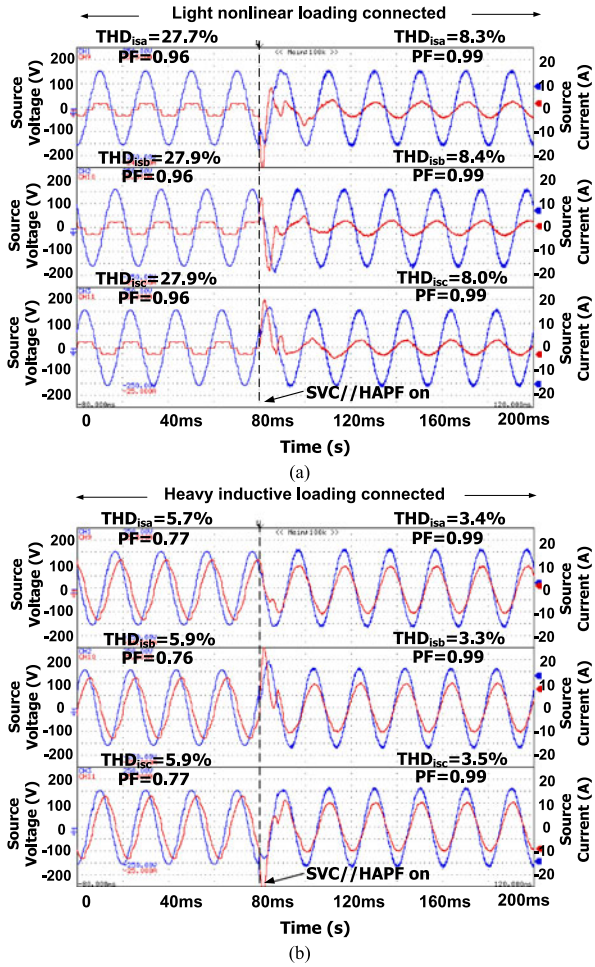

Fig. 10. Waveforms of v_{sx} and i_{sx} by using SVC//HAPF for (a) light nonlinear loading compensation and (b) heavy inductive loading compensation.

TABLE V
EXPERIMENTAL RESULTS FOR DIFFERENT LOADS COMPENSATION BEFORE AND AFTER SVC//HAPF COMPENSATION

			Q_{sx} (var)	PF	i_{sx} (A)	$\mathrm{THD}_{isx}(\%)$	V_{DC}(V)
Light inductive loads	Before Comp.	A	20	0.96	2.1	27.7	–
		B	10	0.96	2.0	27.9	
		C	20	0.96	2.1	27.9	
	SVC//HAPF	A	0	0.99	2.0	8.3	50
		B	10	0.99	2.0	8.4	
		C	10	0.99	2.0	8.0	
Heavy inductive loads	Before Comp.	A	640	0.77	8.7	5.7	–
		B	650	0.76	8.8	5.9	
		C	650	0.77	8.7	5.9	
	SVC//HAPF	A	10	0.99	7.0	3.4	50
		B	10	0.99	6.9	3.3	
		C	10	0.99	7.0	3.5	

Note: The shaded areas mean undesirable results.

performances. As the cost of the SVC part is much lower than that of active inverter part, the reduction of the inverter rating (voltage and current) can lead to a decrease in the total cost of the SVC//HAPF system. Therefore, the SVC//HAPF is a cost-effective solution for medium-voltage-level heavy loads compensation. And, the detailed cost study is given in the Appendix.

VI. EXPERIMENTAL RESULTS

In this section, a 110 V−5 kVA experimental prototype of the SVC//HAPF with the proposed parameter and control design methods is built in the laboratory, as shown in Fig. 9. The digital control system of the SVC//HAPF is digital signal processor (DSP) TMS320F2812, and the sampling frequency of the control system is 25 kHz. For every 1/25 kHz(s) period, the timer will provide a signal to process analog to digital (A/D) conversion and the corresponding interrupt. After processing the control algorithm, the output PWMs signal will be generated and the maximum PWM switching frequency is 12.5 kHz. For both simulation and experiment, the minimum switching frequency is about 0.7 kHz. The switching devices for the active inverter part are Mitsubishi IGBT intelligent power modules PM300DSA060. And the switching devices for the SVC part are thyristors SanRex PK110FG160. Moreover, the experimental parameters of the SVC//HAPF are the same as shown in Table III.

Fig. 10 shows the waveforms of source voltage and current by using the SVC//HAPF for light nonlinear loading compensation and heavy inductive loading compensation. Fig. 11 shows the harmonic spectrums of source current before and after compensation for different loads. Table V summarizes the corresponding experiments results.

From Figs. 10(a) and 11(a) and (b) and Table V, after SVC//HAPF compensation, the worst-phase PF has been compensated from 0.96 to 0.99 for light harmonic loads compensation. The

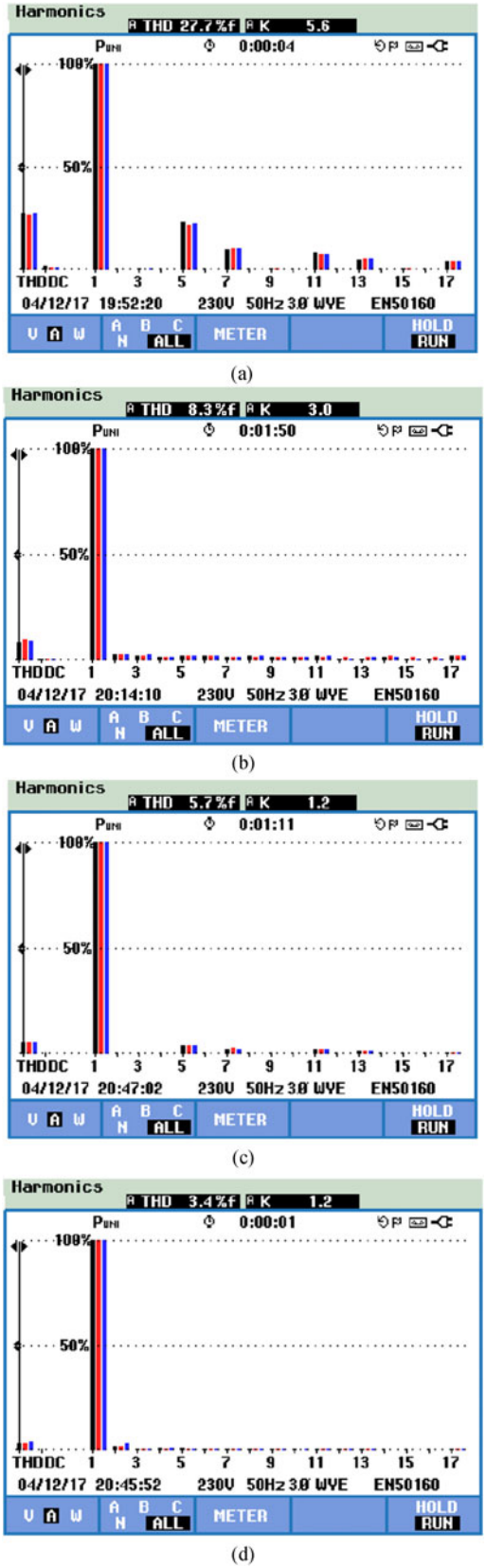

Fig. 11. Harmonic spectrums of source current for light harmonic loading compensation: (a) before SVC//HAPF compensation, (b) after SVC//HAPF compensation; for heavy inductive loading compensation: (c) before SVC//HAPF compensation and (d) after SVC//HAPF compensation.

worst-phase THD_{isx} has been compensated to 8.4% from the original 27.9% for light harmonic loads compensation.

From Figs. 10(b) and 11(c) and (d) and Table V, the proposed SVC//HAPF can compensate the heavy loads situation. The fundamental source reactive power is reduced from 650 var to almost 10 var. And, the PF has been improved from 0.77 to 0.99. Also, the worst-phase THD_{isx} has been compensated to 3.5% from the original 5.9%. Moreover, the source voltage and current are in phase with each other after SVC//HAPF compensation.

VII. Conclusion

In this paper, a new hybrid structure of SVC in parallel with HAPF (SVC//HAPF) in three-phase power system was proposed and discussed as a cost-effective compensator for medium-voltage heavy loads compensation. The SVC part was used to dynamically compensate the reactive power, while the HAPF was used to provide harmonic and low fixed amount of reactive power compensation. Moreover, the structure, modeling, operation principle, parameter design, and control method of the SVC//HAPF were proposed and discussed. Finally, the representative simulation and experimental results were given to show that the SVC//HAPF has the great promise in wide reactive power compensation range with both low-voltage and current inverter rating characteristics.

Appendix

The proposed SVC//HAPF can be considered as SVC in parallel with the combination of PPF in series with APF. The key idea of proposed SVC//HAPF is to share the major compensation power in low cost SVC part and PPF part instead of the high cost APF part. On the other hand, in medium-voltage system, the conventional APFs require multilevel structures to reduce the high voltage stress across each power switch and dc-link capacitor. Thus, compared with the proposed SVC//HAPF, the multilevel APF consists of more components especially for switching devices like IGBTs. Therefore, the reliability of the multilevel APF is lower than the SVC//HAPF, and the control complexity and switching loss of the multilevel APF are higher than SVC//HAPF. Even the proposed SVC//HAPF may have larger size than traditional multilevel APF, the proposed SVC//HAPF has the lower cost than the traditional multilevel APF.

According to the cost study in [20] and [21], the cost of APF is about \$60/kVA. And, the cost of active inverter per kVA (\$/kVA) is much higher than passive power filter (PPF) (∼\$5/kVA) and the SVC (∼\$18/kVA). Therefore, the hybrid system consists of SVC or PPF and low rating active inverter can be considered as a more cost-effective solution than the APFs.

The HAPF can be considered as the PPF in series with APF. And, SVC–HAPF can be considered as the SVC in series with APF. The proposed SVC//HAPF can be considered as SVC in parallel with the combination of PPF in series with APF. The cost of HAPF, SVC–HAPF and the proposed SVC//HAPF can be approximately calculated as

TABLE VI
Cost Comparison of PPF, SVC, APF, HAPF, SVC–HAPF, and the Proposed SVC//HAPF

Compensator	PPF	SVC	APF	HAPF	SVC–HAPF	SVC//HAPF
Cost (\$/kVA)	∼5	∼18	∼60	∼9.5	∼30	∼17.4

$$\mathrm{Cost}_{\mathrm{HAPF}} = \mathrm{Cost}_{\mathrm{PPF}} + k_{\mathrm{HAPF}} \cdot \mathrm{Cost}_{\mathrm{APF}} \tag{27}$$

$$\mathrm{Cost}_{\mathrm{SVC-HAPF}} = \mathrm{Cost}_{\mathrm{SVC}} + k_{\mathrm{SVC-HAPF}} \cdot \mathrm{Cost}_{\mathrm{APF}} \tag{28}$$

$$\mathrm{Cost}_{\mathrm{SVC-HAPF}} = k_{\mathrm{SVC}} \cdot \mathrm{Cost}_{\mathrm{SVC}} + k_{\mathrm{PPF}} \cdot \mathrm{Cost}_{\mathrm{PPF}} + k_{\mathrm{SVC//HAPF}} \cdot \mathrm{Cost}_{\mathrm{APF}} \tag{29}$$

where $\mathrm{Cost}_{\mathrm{PPF}}, \mathrm{Cost}_{\mathrm{APF}}, \mathrm{Cost}_{\mathrm{SVC}}, \mathrm{Cost}_{\mathrm{SVC-HAPF}}$, and $\mathrm{Cost}_{\mathrm{SVC//HAPF}}$ are, respectively, the costs of PPF, APF, SVC, SVC–HAPF, and SVC//HAPF. And, $k_{\mathrm{HAPF}}, k_{\mathrm{SVC-HAPF}}$, and $k_{\mathrm{SVC//HAPF}}$ are the active inverter capacity ratio between APF and HAPF, APF and SVC–HAPF, and APF and SVC//HAPF, respectively. For the SVC//HAPF, since the compensating current are shared by the SVC part and the HAPF part, k_{SVC} and k_{PPF} are the current ratio between the SVC part and the whole system and the HAPF part and the whole system.

According to the case studies in Fig. 8 and Table IV, $k_{\mathrm{HAPF}}, k_{\mathrm{SVC-HAPF}}$, and $k_{\mathrm{SVC//HAPF}}, k_{\mathrm{SVC}}$, and k_{PPF} are $k_{\mathrm{HAPF}} \approx 0.075, k_{\mathrm{SVC-HAPF}} \approx 0.2, k_{\mathrm{SVC//HAPF}} \approx 0.075, k_{\mathrm{SVC}} \approx 0.625$, and $k_{\mathrm{PPF}} \approx 0.375$. Based on the earlier analysis, (27)–(29) and cost study in [20] and [21], the cost of each compensator can be approximately calculated as shown in Table VI.

Based on Table VI, it can be seen that the proposed SVC//HAPF is more cost effective than the conventional APF and SVC–HAPF. Even though the HAPF can obtain lower cost than the SVC//HAPF, it has very narrow reactive power compensation range and cannot provide satisfactory performance for heavy loads compensation as verified by Fig. 8 and Table IV.

References

[1] A. Hamadi, S. Rahmani, and K. Al-Haddad, "A hybrid passive filter configuration for VAR control and harmonic compensation," *IEEE Trans. Ind. Electron.*, vol. 57, no. 7, pp. 2419–2434, Jul. 2010.

[2] L. Wang, C. S. Lam, and M. C. Wong, "Design of a thyristor controlled LC compensator for dynamic reactive power compensation in smart grid," *IEEE Trans. Smart. Grid.*, vol. 8, no. 1, pp. 409–417, Jan. 2017.

[3] J. Chen, X. Zhang, and C. Wen, "Harmonics attenuation and power factor correction of a more electric aircraft power grid using active power filter," *IEEE Trans. Ind. Electron.*, vol. 63, no. 12, pp. 7310–7319, Dec. 2016.

[4] Z. Shu, M. Liu, L. Zhao, S. Song, Q. Zhou, and X. He, "Predictive harmonic control and its optimal digital implementation for MMC-based active power filter," *IEEE Trans. Ind. Electron.*, vol. 63, no. 8, pp. 5244–5254, Aug. 2016.

[5] X. Sun *et al.*, "Study of a novel equivalent model and a long-feeder simulator-based active power filter in a closed-loop distribution feeder," *IEEE Trans. Ind. Electron.*, vol. 63, no. 5, pp. 2702–2712, May 2016.

[6] L. Wang, C. S. Lam, M. C. Wong, N. Y. Dai, K. W. Lao, and C. K. Wong, "Non-linear adaptive hysteresis band pulse-width modulation control for hybrid active power filters to reduce switching loss," *IET Power Electron.*, vol. 8, no. 11, pp. 2156–2167, Nov. 2015.

[7] K. W. Lao *et al.*, "Analysis in the effect of co-phase traction railway HPQC coupled impedance on its compensation capability and impedance-mapping design technique based on required compensation capability for reduction in operation voltage," *IEEE Trans. Power Electron.*, vol. 32, no. 4, pp. 2631–2646, Apr. 2017.

[8] J. Dixon, Y. del Valle M. Orchard, M. Ortuzar, L. Moran, and C. Maffrand, "A full compensating system for general loads, based on a combination of thyristor binary compensator, and a PWM-IGBT active power filter," *IEEE Trans. Ind. Electron.*, vol. 50, no. 5, pp. 982–989, Oct. 2003.
[9] A. Luo, S. Peng, C. Wu, J. Wu, and Z. Shuai, "Power electronic hybrid system for load balancing compensation and frequency-selective harmonic suppression," *IEEE Trans. Ind. Electron.*, vol. 59, no. 2, pp. 723–732, Feb. 2012.
[10] L. Wang, C. S. Lam, and M. C. Wong, "An unbalanced control strategy for a thyristor controlled LC-coupling hybrid active power filter (SVC–HAPF) in three-phase three-wire systems," *IEEE Trans. Power Electron.*, vol. 32, no. 2, pp. 1056–1069, Feb. 2017.
[11] S. Rahmani, A. Hamadi, and K. Al-Haddad, "A combination of shunt hybrid power filter and thyristor-controlled reactor for power quality," *IEEE Trans. Ind. Electron.*, vol. 61, no. 5, pp. 2152–2164, May 2014.
[12] L. Wang, C. S. Lam, and M. C. Wong, "A hybrid-STATCOM with wide compensation range and low dc-link voltage," *IEEE Trans. Ind. Electron.*, vol. 63, no. 6, pp. 3333–3343, Jun. 2016.
[13] L. Wang, C. S. Lam, and M. C. Wong, "Hardware and software design of a low dc-link voltage and wide compensation range thyristor controlled LC-coupling hybrid active power filter," in *Proc. IEEE Reg. 10 Conf.*, Nov. 2015, pp. 1–4.
[14] L. Wang, C. S. Lam, and M. C. Wong, "Modeling and parameter design of thyristor controlled LC-coupled hybrid active power filter (SVC–HAPF) for unbalanced compensation," *IEEE Trans. Ind. Electron.*, vol. 64, no. 3, pp. 1827–1840, Mar. 2017.
[15] C. S. Lam, L. Wang, S. I. Ho, and M. C. Wong, "Adaptive thyristor controlled LC–hybrid active power filter for reactive power and current harmonics compensation with switching loss reduction," *IEEE Trans. Power Electron.*, vol. 32, no. 10, pp. 7577–7590, Oct. 2017.
[16] L. Wang, C. S. Lam, and M. C. Wong, "Analysis, control and design of hybrid grid-connected inverter for renewable energy generation with power quality conditioning," *IEEE Trans. Power Electron.*, vol. PP, no. 99, 2017, doi: 10.1109/TPEL.2017.2753838.
[17] L. Wang, C. S. Lam, and M. C. Wong, "Delta-connected static var compensator (SVC) based hybrid active power filter (SVC–HAPF) and its control method," presented at the *43rd Annu. Conf. IEEE Ind. Electron. Soc.*, Beijing, China, Oct. 29–Nov. 01, 2017.
[18] L. Wang, C. S. Lam, and M. C. Wong, "Selective compensation of distortion, unbalanced and reactive power of a thyristor controlled LC-coupling hybrid active power filter (SVC–HAPF)," *IEEE Trans. Power Electron.*, vol. 32, no. 12, pp. 9065–9077, Dec. 2017.
[19] H. Akagi, Y. Kanazawa, and A. Nabae, "Instantaneous reactive power compensators comprising switching devices without energy storage components," *IEEE Trans. Ind. Appl.*, vol. IA-20, no. 3, pp. 625–630, May 1984.
[20] K. W. Lao, M. C. Wong, N. Dai, C. K. Wong, and C. S. Lam, "A systematic approach to hybrid railway power conditioner design with harmonic compensation for high-speed railway," *IEEE Trans. Ind. Electron.*, vol. 62, no. 2, pp. 930–942, Feb. 2015.
[21] K. W. Lao, N. Dai, W. G. Liu, and M. C. Wong, "Hybrid power quality compensator with minimum dc operation voltage design for high-speed traction power systems," *IEEE Trans. Power. Electron.*, vol. 28, no. 4, pp. 2024–2036, Apr. 2013.
[22] S. Srianthumrong and H. Akagi, "A medium-voltage transformerless AC/DC power conversion system consisting of a diode rectifier and a shunt hybrid filter," *IEEE Trans. Ind. Appl.*, vol. 39, no. 3, pp. 874–882, May–Jun. 2003.
[23] C. S. Lam, M. C. Wong, and Y. D. Han, "Hysteresis current control of hybrid active power filters," *IET Power Electron.*, vol. 5, no. 7, pp. 1175–1187, Aug. 2012.

Lei Wang received the B.Sc. degree in electrical and electronics engineering from University of Macau (UM), Macao, China, in 2011, the M.Sc. degree in electronics engineering from Hong Kong University of Science and Technology (HKUST), Hong Kong, China, in 2012, and the Ph.D. degree in electrical and computer engineering from UM in 2017.

He is currently a Postdoctoral Fellow in the Power Electronics Laboratory, UM. His current research interests include power electronics, power quality and distribution flexible ac transmission system (DFACTS), power quality compensation, and renewable energy.

Dr. Wang was the recipient of the champion award in the "Schneider Electric Energy Efficiency Cup," Hong Kong, 2011.

Chi-Seng Lam (S'04–M'12–SM'16) received the B.Sc., M.Sc., and Ph.D. degrees in electrical and electronics engineering from the University of Macau (UM), Macao, China, in 2003, 2006 and 2012, respectively.

From 2006 to 2009, he was an Electrical and Mechanical Engineer with UM. From 2009 to 2012, he was a Laboratory Technician with UM. In 2013, he was a Postdoctoral Fellow in The Hong Kong Polytechnic University, Hong Kong, China. He is currently an Assistant Professor with the State Key Laboratory of Analog and Mixed Signal VLSI, UM. He has authored or coauthored two Springer books (2014, 2016) and more than 60 technical journal and conference papers. His current research interests include integrated controllers, power management integrated circuits, power quality compensators, smart grid technology, renewable energy, etc.

Dr. Lam is a Vice-Chair of the IEEE Macau Section and a Chair of IEEE Macau CAS/COM Joint Chapter. He was the recipient of the IEEE Power and Energy Society (PES) Chapter Outstanding Engineer Award in 2016; the Macao Science and Technology Invention Award (Third Class) and the R&D Award for Postgraduates (Ph.D. Level) in 2014 and 2012, respectively; and the RIUPEEEC Merit Paper Award in 2005.

Man-Chung Wong (SM'06) received the B.Sc. and M.Sc. degrees in electrical and electronics engineering from the University of Macau (UM), Macao, China, in 1993 and 1997, respectively, and the Ph.D. degree in electrical engineering from Tsinghua University, Beijing, China, in 2003.

From July 2014 to December 2014, he was a Visiting Fellow at the University of Cambridge, Cambridge, U.K. He is currently an Associate Professor with the Department of Electrical and Computer Engineering, University of Macau. His current research interests include power electronics converters, pulsewidth modulation, active power filters, hybrid active power filters, etc. He has authored or coauthored two Springer books and over 100 journal and conference papers.

Dr. Wong was the recipient of the Young Scientist Award from the "Instituto Internacional De Macau" in 2000, the Young Scholar Award from the University of Macau in 2001, the second prize of the Tsinghua University Excellent Doctor Thesis Award in 2003, and the third prize award of the Invention Award of the Macau Government Science and Technology Award in 2012 and 2014.